



**HAL**  
open science

## Topoisomerase VI participates in an insulator-like function that prevents H3K9me2 spreading

Louis-Valentin Meteignier, Cécile Lecampion, Florent Velay, Cécile Vriet, Laura Dimnet, Martin Rougée, Christian Breuer, Ludivine Soubigou-Tacconnat, Keiko Sugimoto, Fredy Barneche, et al.

► **To cite this version:**

Louis-Valentin Meteignier, Cécile Lecampion, Florent Velay, Cécile Vriet, Laura Dimnet, et al.. Topoisomerase VI participates in an insulator-like function that prevents H3K9me2 spreading. Proceedings of the National Academy of Sciences of the United States of America, 2022, 119 (27), 10.1073/pnas.2001290119 . hal-03862125

**HAL Id: hal-03862125**

**<https://cnrs.hal.science/hal-03862125>**

Submitted on 28 Nov 2022

**HAL** is a multi-disciplinary open access archive for the deposit and dissemination of scientific research documents, whether they are published or not. The documents may come from teaching and research institutions in France or abroad, or from public or private research centers.

L'archive ouverte pluridisciplinaire **HAL**, est destinée au dépôt et à la diffusion de documents scientifiques de niveau recherche, publiés ou non, émanant des établissements d'enseignement et de recherche français ou étrangers, des laboratoires publics ou privés.



Distributed under a Creative Commons Attribution - NonCommercial - NoDerivatives 4.0 International License

1 **Topoisomerase VI participates in an insulator-like function that prevents H3K9me2**  
2 **spreading.**

3

4 Louis-Valentin Méteignier<sup>1</sup>, Cécile Lecampion<sup>1</sup>, Florent Velay<sup>1</sup>, Cécile Vriet<sup>1,2</sup>, Laura Dimnet<sup>1</sup>, Michel  
5 Térése<sup>3</sup>, Martin Rougée<sup>4,5</sup>, Christian Breuer<sup>6</sup>, Ludivine Soubigou-Taconnat<sup>7,8</sup>, Keiko Sugimoto<sup>6</sup>, Fredy  
6 Barneche<sup>4,5</sup> and Christophe Laloi<sup>1\*</sup>.

7

8 <sup>1</sup>Aix Marseille Univ, CEA, CNRS, BIAM, Marseille, France F-13009

9 <sup>2</sup>UMR CNRS 7267, University of Poitiers, 86073 Poitiers Cedex

10 <sup>3</sup>Independent informatician, 06100 Nice, France

11 <sup>4</sup>IBENS, Département de Biologie, Ecole Normale Supérieure, CNRS, PSL Research University, F-  
12 75005, Paris, France

13 <sup>5</sup>Université Paris-Sud, Université Paris-Saclay, 91405, Orsay, France.

14 <sup>6</sup>RIKEN Center for Sustainable Resource Science, Yokohama, 230-0045, Japan

15 <sup>7</sup>Institute of Plant Sciences Paris Saclay IPS2, CNRS, INRA, Université Paris-Sud, Université Evry,  
16 Université Paris-Saclay, Bâtiment 630, 91405 Orsay, France.

17 <sup>8</sup>Institute of Plant Sciences Paris-Saclay IPS2, Paris Diderot, Sorbonne Paris-Cité, Bâtiment 630,  
18 91405, Orsay, France

19

20 **Corresponding author:**

21 Christophe Laloi, [christophe.laloi@univ-amu.fr](mailto:christophe.laloi@univ-amu.fr)

22

23 **Classification:**

24 BIOLOGICAL SCIENCES: Plant Biology

25

26 **Keywords**

27 Euchromatin islands / Heterochromatin spreading / Insulator / Methionine Adenosyltransferase /  
28 Topoisomerase VI.

29

30 **Abstract**

31 The organization of the genome into transcriptionally active and inactive chromatin domains requires  
32 well-delineated chromatin boundaries and insulator functions in order to maintain the identity of  
33 adjacent genomic loci with antagonistic chromatin marks and functionality. In plants that lack known  
34 chromatin insulators, the mechanisms that prevent heterochromatin spreading into euchromatin  
35 remain to be identified. Here, we show that DNA Topoisomerase VI participates in a chromatin  
36 boundary function that safeguards the expression of genes in euchromatin islands within silenced  
37 heterochromatin regions. While some transposable elements are reactivated in mutants of the  
38 Topoisomerase VI complex, genes insulated in euchromatin islands within heterochromatic regions  
39 of the *Arabidopsis thaliana* genome are specifically downregulated. H3K9me2 levels consistently  
40 increase at euchromatin island loci and decrease at some TE loci. We further show that  
41 Topoisomerase VI physically interacts with S-adenosylmethionine (SAM) synthase MAT3, which is  
42 required for H3K9me2. A Topoisomerase VI defect affects MAT3 occupancy on heterochromatic  
43 elements and its exclusion from euchromatic islands, thereby providing a possible mechanistic  
44 explanation to the essential role of Topoisomerase VI in the delimitation of chromatin domains.

45

46 **Significance Statement**

47 In the eukaryotic genome, DNA associates with proteins and form two main types of chromatin, the  
48 highly condensed heterochromatin, which is inaccessible to transcription factors and hence  
49 transcriptionally silent, and the less condensed, hence transcriptionally active euchromatin. The  
50 maintenance of sharp boundaries between these chromatin domains with antagonistic functionality  
51 is therefore critical for transcriptional control and involves chromatin insulators that remain  
52 unknown in plants. Here, we show that a plant topoisomerase participates in such a chromatin  
53 boundary function that prevent heterochromatin spreading into euchromatin and hence safeguards  
54 the expression of genes in euchromatin islands within silenced heterochromatin regions. We have  
55 also identified partners of this topoisomerase that allow us to provide a mechanistic insight to this  
56 insulator-like function.

57

## 58 Introduction

59           The discovery of position effect variegation in *Drosophila melanogaster* paved the way  
60 towards revealing the importance of chromatin contexts in the regulation of gene expression (1, 2).  
61 Since then, cytogenetic and molecular profiling of the epigenome, as well as topological analyses of  
62 chromatin architecture, have allowed the mechanisms involved in partitioning the gene-rich  
63 euchromatic fraction from the repeat-rich heterochromatic fraction to be elucidated. Large protein  
64 complexes specific to insulator DNA sequences contribute to partitioning chromatin domains with  
65 distinct identity at multiple scales. These complexes maintain the identity of adjacent genomic loci  
66 with antagonistic chromatin marks and functionality, and more globally influence the formation of  
67 long-range chromosomal interactions (3). Insulator binding proteins such as the CCCTC-binding factor  
68 CTCF, BEAF-32, CP190 and Mod have been best described in *Drosophila* where they play critical roles  
69 in the definition of chromatin and transcriptional status. In vertebrates, CTCF is the only known  
70 insulator binding protein homologue. CTCF is enriched at insulator DNA sequences that define large  
71 topological domains of the genome (4–6) and, in some cases, define boundaries between adjacent  
72 chromatin domains with distinct features (7). Surprisingly, CTCF orthologs cannot be identified in  
73 many eukaryotic organisms, including plants (8). Moreover, very few studies support the presence of  
74 insulator DNA sequences or insulator-like regions in plants (9–11), and insulator binding factors  
75 remain to be identified. This contrasts with the observation that *Arabidopsis thaliana* and other plant  
76 species display highly indexed chromatin states along the genome, with well-defined chromatin  
77 signatures around transcriptionally active or repressed genes, as well as close relationships between  
78 chromatin composition and genome topology in the nuclear space (12, 13). In *Arabidopsis*,  
79 heterochromatin is found on hundreds of transposable elements (TEs) mostly confined within the  
80 pericentromeric regions and at a few knob structures that tend to associate through long-distance  
81 interactions in the nuclear space (14–18). As a result, in *Arabidopsis* interphase nuclei most  
82 cytologically visible heterochromatin is condensed within 8 to 10 conspicuous foci that are referred  
83 to as chromocenters (19–21). Consistent with their heterochromatic nature, chromocenters are  
84 refractory to transcription and contain highly methylated DNA (22) as well as histone modifications  
85 such as H3K9me2 and H3K27me2 (23, 24). Nonetheless, many expressed genes exhibiting  
86 euchromatic features appear to be located in close vicinity to large heterochromatic regions in the  
87 *Arabidopsis* genome, notably within the pericentromeric and knob regions (25, 26). The mechanisms  
88 by which gene-containing euchromatic islands (EIs) are insulated from neighboring heterochromatin  
89 regions and how their transcriptional capacities are preserved in such chromatin contexts are largely  
90 unknown. In this study, we have unveiled an essential function of the plant Topoisomerase VI  
91 complex in preserving the functional and structural identity of EIs.

92 DNA topoisomerases are enzymes that introduce transient DNA breaks to resolve topological  
93 constraints that arise during multiple cellular processes such as replication, transcription,  
94 recombination and chromatin remodeling. The plant Topo VI, a type II topoisomerase first identified  
95 in the archaeon *Sulfolobus shibatae* (27, 28), was initially implicated in various biological processes  
96 involving endoreduplication, such as root hair growth (29–31), hypocotyl elongation (31) and nodule  
97 differentiation (32). Topo VI forms an A<sub>2</sub>B<sub>2</sub> heterotetramer whose A and B subunits are encoded by  
98 single genes in *Arabidopsis*, *AtTOP6A/CAA39/AtSPO11-3/RHL2/BIN5/AT5G02820* and  
99 *AtTOP6B/RHL3/BIN3/HYP6/HLQ/AT3G20780*, respectively (33–37). Two additional subunits named  
100 ROOT HAIRLESS 1 (RHL1/HYP7/AT1G48380) and BRASSINOSTEROID-INSENSITIVE 4  
101 (BIN4/MID/AT5G24630) (31, 38, 39) are essential for the *Arabidopsis* Topo VI function and appear to  
102 be evolutionarily conserved in plants and in other eukaryote groups, whilst their precise functions  
103 remain unclear. However, BIN4 shares sequence similarity with the C-terminal region of animal Topo  
104 II $\alpha$ , which seems to have regulatory functions (40–42), and exhibits stable DNA binding *in vitro* (38).  
105 Therefore, it has been proposed that BIN4 may have a regulatory role in the plant Topo VI complex,  
106 presumably by holding the substrate DNA through its AT-hook motif (38, 39).

107 In recent years, evidence has accumulated that topoisomerases have more diverse and  
108 specialized functions than previously thought (43). In particular, transcriptomic analyses of several  
109 Topo VI mutants revealed that Topo VI influences the expression of many nuclear genes, including  
110 genes regulated by phytohormones (35, 36) or by reactive oxygen species (44–46). A function of  
111 *Arabidopsis* Topo VI as a chromatin-remodeling complex has also been speculated (35). This  
112 hypothesis has since been supported by the observation that loss of the Topo VI B subunit in *hlq*  
113 mutant plants leads to the mis-expression of numerous adjacent genes, hence possibly triggering  
114 positional or chromatin context dependent transcriptional defects (36). This is further supported by  
115 the implication of the BIN4 subunit in heterochromatin organization, as observed by smaller and  
116 diffuse chromocenters in interphase nuclei of plants bearing the severe *mid* mutation (39).

117 Here, we reveal that *Arabidopsis* Topo VI is required for chromocenter formation and for  
118 efficient silencing of some heterochromatic TEs but has an antagonistic effect on genes localized in  
119 euchromatic islands (EIs). Downregulation of EI genes in Topo VI mutant plants is associated with an  
120 enrichment of the H3K9me2 heterochromatic mark. We further report that the BIN4 subunit of Topo  
121 VI directly interacts with S-adenosylmethionine (SAM) synthetase 3 / Methionine Adenosyl  
122 transferase 3 (MAT3). Similar to Topo VI knockdown plants, *mat3* knockdown mutants exhibit de-  
123 repression of heterochromatic TEs and a decrease in H3K9me2. Furthermore, we show that the  
124 association of MAT with heterochromatic elements is reduced in a hypomorphic Topo VI mutant,  
125 whereas it increased at some EIs. We therefore propose that Topo VI has a prominent role in the

126 delimitation of chromatin boundaries, could participate in defining SAM synthesis sites onto specific  
127 regions of the genome, and collectively has an essential role in the establishment of distinct  
128 chromatin domains.

129

## 130 **Results**

### 131 **Topoisomerase VI is required for heterochromatin organization**

132 Kirik *et al.* reported that interphase nuclei of the severe *mid* mutant in the BIN4/MID subunit  
133 presents smaller and less defined chromocenters (CCs) compared to the wild-type (wt), suggesting  
134 that heterochromatin organization is affected by the *mid* mutation (39). However, this phenotype  
135 was not reported in the allelic *bin4-1* mutant, which also has a severe phenotype (38). Therefore, to  
136 unequivocally confirm the role of the *Arabidopsis* Topo VI complex in nuclear organization, we  
137 analyzed the nuclear phenotypes of hypomorphic and amorphic mutants of the AtTOP6A subunit,  
138 *caa39* and *rhl2-1*, and of the BIN4/MID subunit, a *BIN4* knockdown line (*BIN4* KD, see below) and  
139 *bin4-1*, by DAPI DNA staining and immunolocalization of heterochromatin hallmarks. Both the *caa39*  
140 and *rhl2-1* mutants exhibited strong alterations in heterochromatin organization with largely  
141 decondensed chromocenters (Fig 1A, top panel, and SI Appendix, Fig S1A). Likewise, nuclei of  
142 epidermal and mesophyll cotyledon cells from *BIN4* KD and *bin4-1* did not harbor conspicuous  
143 chromocenters (SI Appendix, Fig S1A), as previously reported for the *mid* allelic mutants (39). In  
144 contrast, the nuclear phenotype of shoot apical meristematic cells is similar in wt, *caa39*, *rhl2-1*,  
145 *bin4-1* and *BIN4* KD lines, with equal proportions of nuclei with conspicuous (type 1) or diffuse (type  
146 2) chromocenter profiles (SI Appendix, Fig S1A, meristem panel, and Fig S1B). Consistent with its role  
147 in endocycles but not in mitosis (31, 37–39), these defects indicate that Topo VI is required for  
148 chromatin organization of differentiated cells, but less of actively dividing cells. Immunofluorescence  
149 analysis of the heterochromatin hallmark H3K9me2 confirmed the large extent of heterochromatin  
150 decondensation in *caa39* Topo VI mutant plants (Fig 1A). Immunoblot analyses further showed that  
151 the global level of H3K9me2 is not affected in *caa39* seedlings (Fig 1B). Likewise, 5-methylcytosine (5-  
152 meC) immunolabeling also revealed a dispersed signal in *caa39* nuclei (Fig 1C) whereas an anti-5-meC  
153 ELISA showed overall similar levels of 5-meC in wt and *caa39* as compared to *ddm1-8* seedlings (Fig  
154 1D). These results suggest that the marked alteration of chromocenter morphology does not result  
155 from a global decrease in heterochromatin hallmarks in *caa39*.

156

### 157 **Topo VI is required for the silencing of heterochromatic transposable elements**

158 A role for *Arabidopsis* Topo VI in heterochromatin-dependent transcriptional gene silencing  
159 was highlighted by the reactivation of *TRANSCRIPTIONALLY SILENT INFORMATION (TSI)* in *mid* mutant  
160 plants (39). However, reactivation was not observed in the *bin4-1* allelic mutant (38). Therefore, to  
161 unambiguously assess the involvement of Topo VI in transcriptional silencing and get a more global  
162 understanding of Topo VI influence on TE repression, we performed a RNA-seq analysis of *caa39* and  
163 wt transcripts. Multiple heterochromatic TEs (176 TEs with  $\log_2(\text{FC}) > 2$ ), particularly from the  
164 LTR/Gypsy, LTR/Copia and En-Spm/CACTA superfamilies (47), are reactivated in *caa39* plants (Fig 2A,  
165 Dataset S1). Conversely, 91 TEs are repressed in *caa39* ( $\log_2(\text{FC}) < -2$ ); unlike reactivated TEs, these  
166 repressed TEs are rarely in the most inaccessible and repressive heterochromatin state 9 (SI  
167 Appendix, Fig S2A). To test for TE silencing defects in other Topo VI mutants, we selected several de-  
168 repressed heterochromatic TEs loci (Dataset S1) for which robust primer design was feasible, and  
169 measured their relative transcript abundance by RT-qPCR in *rh12-1* and *bin4-1* mutants along with the  
170 *caa39* and wt lines. A clear increase in TE transcript abundance was observed for all three tested  
171 Topo VI mutant lines (Fig 2B).

172 Although we found no global decrease of H3K9me2 and 5-meC in *caa39* (Fig 1B and 1D),  
173 more subtle local changes could account for TE reactivation. We first assessed DNA methylation  
174 levels at individual TEs in Topo VI mutants as compared to wt and *ddm1-8* plants by digestion with  
175 the methylation-dependent restriction enzyme McrBC. As expected, very efficient digestion of TEs  
176 was observed in wt but not in *ddm1-8* plants, reflecting a nearly complete loss of DNA methylation  
177 over multiple TEs in this hypomethylated mutant line (Fig 2C). In sharp contrast, we observed wt  
178 levels of DNA methylation for all tested loci in *caa39* and *bin4-1* plants. This trend was confirmed in  
179 different sequence contexts (CG, CHG and CHH) by using the methylation-sensitive restriction  
180 enzymes HpaII, MspI and HaeIII (SI Appendix, Fig S3). Similar DNA methylation levels of TEs in wt and  
181 *caa39* were then confirmed genome-wide by whole-genome bisulfite sequencing, in all three  
182 contexts (Fig 2D). We concluded that TE de-repression in Topo VI mutants could not be accounted for  
183 by a global decrease of DNA methylation in *cis*. Next, we measured the level of H3K9me2 at TEs,  
184 which could be performed only with the *caa39* hypomorphic mutant, owing to the extreme dwarf  
185 phenotype of the *rh12-1* and *bin4-1* null mutants. ChIP-qPCR analyses revealed a modest decrease in  
186 H3K9me2 at some but not all tested TEs in *caa39* as compared to wt plants (Fig 2E). ChIP-seq analysis  
187 of H3K9me2 levels in wt and *caa39*, normalized to H3 levels in each line, confirmed the slight  
188 decrease of H3K9me2 at *AT3TE60425* and *AT4TE15030*, but not at *AT2TE15415* and *AT4TE16900* (SI  
189 Appendix, Fig S2B-C), and revealed a significant global decrease ( $P < 0.01$ , Mann-Whitney test) of  
190 H3K9me2 at TEs (Fig 2F). Collectively, these results suggest that H3K9me2 local decreases and

191 heterochromatin spatial reorganization may contribute to TE activation, although the precise causal  
192 mechanism is unknown.

193

194 **Unlike TEs, genes interspersed within pericentromeric and chromosome 4 knob large**  
195 **heterochromatin regions are massively downregulated in Topo VI mutants**

196 We then used the online positional gene enrichment tool (48) to investigate the genomic  
197 distribution of misregulated genes identified in our RNA-seq analysis of *caa39* (Dataset S2). This  
198 analysis revealed that the 500 most downregulated genes are strikingly over-represented in  
199 pericentromeric regions (PRs) and in the heterochromatic knob of chromosome 4 (*hk4S*, Fig 3A). In  
200 these regions, 94% (181/193) of the non-TE genes that are differentially expressed in *caa39* are  
201 downregulated (Dataset S2). In contrast, the 500 most highly upregulated genes displayed no  
202 preferential localization (SI Appendix, Fig S4A). To determine whether this effect is robust in other  
203 Topo VI mutant lines, we first examined the expression profiles of *bin4-1* and a second allelic mutant,  
204 *bin4-2*, from microarray data that were generated during the initial characterization of these two  
205 allelic lines (38). Despite the fact that *bin4-1* and *bin4-2* are knock-out mutants that have much more  
206 severe developmental defects than *caa39*, and although two different technical platforms have been  
207 used (RNA-seq for *caa39* vs Affymetrix ATH1 microarrays for *bin4-1* and *bin4-2*), we found a good  
208 correlation between the different transcriptomes (SI Appendix, Fig S4B). In particular, 91% (72/79) of  
209 the PR genes that are repressed in *caa39* and are detected in both RNA-seq and microarray  
210 experiments are also downregulated in *bin4-1* or *bin4-2* (Fig 3B, Dataset S2). We examined further  
211 the expression of seven pericentromeric genes distributed over the five chromosomes and strongly  
212 repressed in *caa39*, by RT-qPCR in *caa39*, *bin4-1* as well as in *rhl2-1* plants. These genes were found  
213 to be downregulated in all mutants, except for *AT4G06634* and *AT4G07390* that were not  
214 significantly repressed in *rhl2-1* and *bin4-1* (Fig 3C). This could possibly be due to secondary effects of  
215 the *bin4-1* and *rhl2-1* amorphic mutations as compared to the less severe *caa39* mutation. In order  
216 to test this hypothesis, we took advantage of the availability of an *Arabidopsis* *BIN4* co-suppressed  
217 transgenic line identified during the process of generating lines overexpressing *BIN4-CFP*. Rather than  
218 exhibiting *BIN4* upregulation, this *BIN4* KD homozygous, mono-insertional transgenic line, shows  
219 downregulation of *BIN4* (SI Appendix, Fig S5A-B) and develops a phenotype similar to *caa39* (SI  
220 Appendix, Fig S5C). In this line, all tested pericentromeric genes were at least as much  
221 downregulated as in *caa39*, with a more pronounced effect than in the *bin4-1* and *rhl2-1* knockout  
222 mutants (Fig 3C). These observations indicate that Topoisomerase VI is required to maintain



223 transcriptional control of both genes and TEs in pericentromeric and *hk4S* regions, possibly acting as  
224 a chromatin architectural factor.

225

## 226 **Downregulated genes within heterochromatic regions are localized in small euchromatic islands**

227 We then asked whether the inverse expression patterns of genes and TEs in pericentromeric  
228 and *hk4S* regions in Topo VI mutants could be ascribed to their different chromatin landscapes. We  
229 first inspected the individual chromatin landscape of the seven downregulated pericentromeric  
230 genes confirmed by RT-qPCR (Fig 3C), using the nine chromatin states defined by Sequeira-Mendes *et*  
231 *al.* (49). Euchromatin states 2, 1 and 3 characterize the proximal promoter, the transcriptional start  
232 site, and the start of coding sequence, respectively. The intragenic states 6 and 7 are characteristic of  
233 the transcriptional termination site and gene body of long transcribed genes, respectively. States 4  
234 and 5 are highly enriched in H3K27me3 (a *Polycomb*-Repressive Complex 2 (PRC2)-based repressive  
235 histone modification) and are usually found in intergenic regions and PRC2-targeted genes. Lastly,  
236 the two types of heterochromatin states, 8 and 9, are enriched in H3K9me2, but in contrast with  
237 state 8, state 9 preferentially defines pericentromeric heterochromatin and is devoid of H3K27me3  
238 (49). Strikingly, all inspected loci share common features: a typical euchromatin context whose  
239 proximal environment is composed of heterochromatic state 8 and whose distal environment is of  
240 heterochromatic state 9 (SI Appendix, Fig S6A). Overall, these observations suggested that *caa39*  
241 downregulated genes might be part of *bona fide* euchromatic islands (EIs).

242 To generate a comprehensive view of their structural features in the genome, we  
243 systematically investigated the pericentromeric and *hk4S* heterochromatic regions defined in  
244 Appendix Figure S6B. We designed a script to extract all EIs surrounded by chromatin states 8 and 9,  
245 then we analyzed the proportion of chromatin states covering EIs and their 1.5 kb flanking regions  
246 (Fig 3D). We identified 232 EIs containing 540 EI genes this way, among which 6 correspond to  
247 unsequenced gaps (<https://jbrowse.arabidopsis.org/?data=Araport11>) and were discarded in  
248 subsequent analyses (Dataset S3). Looking for EIs directly flanked by state 9 chromatin did not  
249 increase the number of EIs identified, showing that chromatin state 8 is always present in the  
250 proximal border (Fig 3D, SI Appendix, Fig S6C). In contrast, the number of detected EIs started to  
251 decrease to 215 when considering two-nucleosome-long flanking regions in state 8, suggesting that  
252 11 EIs have only one proximal nucleosome in state 8 (SI Appendix, Fig S6C). With respect to state 9,  
253 the number of extracted islands began to drop from 4-nucleosome-long flanking regions, suggesting  
254 that the state 8 proximal border is always flanked by at least 3-nucleosome-long state 9 regions (SI

255 Appendix, Fig S6C). A majority of EIs (157/232) are short and contain only one or two genes (Fig. 3E,  
256 Dataset S3, SI Appendix, Table S1).

257

### 258 **Topo VI prevents the spreading of H3K9me2 into euchromatic islands**

259         Given the general repression of EI genes and the local decrease of H3K9me2 at some TE loci  
260 without affecting the global level of H3K9me2 (Fig 1B), we hypothesized that EI gene repression  
261 might result from ectopic spreading of this silencing mark over EIs. This was first tested on several EI  
262 genes by ChIP-PCR analysis of H3K9me2 levels in wt and *caa39*. H3K9me2 levels were very low,  
263 barely above background, in wt, consistent with the fairly high level of expression of these genes (Fig  
264 4A). In contrast, a clear increase of H3K9me2 was observed in *caa39* (Fig 4A). Therefore, we further  
265 tested the spreading of H3K9me2 over EIs on a genome-wide scale by ChIP-seq analysis of H3K9me2  
266 levels in wt and *caa39*, normalized to H3 levels in each line. Analysis of the wt profile showed short  
267 EIs (S-EIs, which contain only one or two genes and are < 6kb-long) with sharp boundaries and where  
268 H3K9me2 was barely detected, flanked by regions with high H3K9me2 levels (Fig 4B). Consistent with  
269 the minor decrease observed only on some TEs presented in Figure 2, the H3K9me2 level is globally  
270 not lower in EI-flanking sequences in *caa39* as compared to wt. In contrast, a clear increase was  
271 observed within S-EIs of *caa39*, which was highly significant all along S-EIs (Mann-Whitney test,  
272 Benjamini-corrected  $P < 0.01$ ), suggesting that Topo VI prevents H3K9me2 spreading across natural  
273 boundaries (Fig 4B). H3K9me2 spreading into large and more complex EIs (L-EIs, > 6kb-long and often  
274 containing internal state 8) was also highly significant and particularly pronounced on L-EIs  
275 boundaries (Fig. 4C). Inspection of meta-profiles for each chromosome confirmed highly significant  
276 H3K9me2 spreading into EIs (SI Appendix, Fig S7A), that was observed for all replicates (SI Appendix,  
277 Fig S7B).

278         To further strengthen our analysis, we applied diffReps (50) on each replicate individually to  
279 confirm differential enrichment of H3K9me2 in EIs of *caa39* and wt (Dataset S4). This very stringent  
280 and not very sensitive analysis (essentially due to the fact that H3K9me2 peaks were barely  
281 detectable in wt and that H3K9me2 spreading does not appear to be sequence-specific) could still  
282 reveal increased levels of H3K9me2 in some EIs of *caa39*, but not all (92.0% in replicate 2, 73.9% in  
283 replicate 3, 27.4% in replicate 1; Dataset S3). The limited number of EIs identified this way in replicate  
284 1 can be attributed to the fact that it was less deeply sequenced than replicates 2 and 3 (GSE103924).  
285 Despite that, there was a large overlap between replicates: among EIs that showed increased levels  
286 of H3K9me2 in *caa39*, only one was identified in replicate 1 but not in replicates 2 or 3, and 96.4%  
287 (161/167) of the EIs identified in replicate 3 were also identified in replicate 2 (SI

288 Appendix, Fig S7C, Dataset S3). We then extracted the number of significantly (diffReps G-test,  $P <$   
289 0.01) up or down H3K9me2 peaks in *caa39* versus wt, in each individual replicate (Dataset S4, sheet  
290 4). A similar percentage of significantly up or down H3K9me2 peaks was observed at the genome  
291 scale by this method (Fig 4D), in agreement with the fact that the global level of H3K9me2 does not  
292 seem to be significantly affected in *caa39*. In contrast, the proportion of peaks was significantly  
293 shifted toward gains of H3K9me2 within EIs, particularly within EI genes and their 5' UTRs (Fig 4D,  
294 Dataset S4), confirming the specific role of Topo VI in safeguarding EI genes from ectopic spreading of  
295 H3K9me2.

296 Globally, these data show that Topo VI is required to prevent elevated H3K9me2 levels within  
297 EIs, presumably by preserving sharp boundaries between these insulated elements to avoid  
298 pervasive spreading of heterochromatin from flanking regions. We further documented such a  
299 barrier-like function on a S-EI containing a single gene, *At1g41830*, by ChIP-qPCR analysis of  
300 H3K9me2. Scanning of six different loci along this region (Fig 4E) in independent experiments  
301 confirmed the increased H3K9me2 levels within the island body, but also a decrease in one  
302 neighboring heterochromatic border (Fig 4E), similarly to what was observed in the ChIP-seq  
303 experiment replicates for this EIs (Fig 4I and SI Appendix, Fig S8) and other inspected EIs (SI Appendix,  
304 Fig S8).

305

### 306 **EI gene repression is correlated with H3K9me2 spreading**

307 We then tried to evaluate the relative contribution of H3K9me2 increase to the  
308 downregulation of EI genes, compared to other heterochromatin and repressive marks. Firstly,  
309 because H3K9me2 and non-CG (CHG and CHH) DNA methylation are strongly inter-dependent (51),  
310 we tested whether H3K9me2 spreading into EIs might in turn, or reciprocally, affect DNA  
311 methylation. Whole-genome bisulfite sequencing revealed that DNA methylation levels in all  
312 sequence contexts were overall unaltered in *caa39* relative to wt in EIs (Fig 4F and I, SI Appendix, Fig  
313 S8). Differentially methylated region (DMR) analyses confirmed that there was no global significant  
314 increase of DNA methylation in EIs (Dataset S5). Surprisingly, despite CHGs being known to be  
315 methylated through a feedback loop with H3K9me2, DMR analyses rather revealed a very slight  
316 decrease of CHG, with 51 hypo-CHG DMRs and 16 hyper-CHG DMRs observed in EIs of *caa39* (with  
317 differences in the methylation percentage higher than 10%,  $P < 0.05$ , Dataset S5). Therefore, DNA  
318 methylation does not seem to contribute to the downregulation of gene expression in EIs.

319 Secondly, because EI boundaries are enriched in H3K27me3-marked heterochromatin state  
320 8, and that H3K27me3 is also found on the proximal promoter (chromatin state 2) and transcribed

321 region of many euchromatic genes (chromatin state 5, silenced genes) (49), we also performed a  
322 genome-wide H3K27me3 analysis by CHIP-seq. Interestingly, we observed a globally inverted  
323 tendency as compared to H3K9me2 profiles: average H3K27me3 levels were locally and significantly  
324 decreased within EIs (SI Appendix, Fig S9A-B). We further documented such a local decrease of  
325 H3K27me3 on the S-EI containing *At1g41830*, by CHIP-qPCR (SI Appendix, Fig S9C). Consistent with  
326 this, K-means linear clustering revealed that H3K27me3 decrease could not be generalized to all EIs,  
327 as it marks only a small subset of EIs in wt (Fig 4G). Thus, H3K27me3 does not seem to contribute to  
328 the global downregulation of EI genes, and its local decrease at some EI genes might even  
329 counterbalance the effect of H3K9me2 increase in a few EIs.

330 Finally, we directly compared EI gene expression with H3K9me2 changes. A vast majority  
331 (90%) of EI genes that show significant changes ( $P < 0.05$ ) in either RNA-seq or CHIP-seq analyses are  
332 repressed and possess enhanced levels of H3K9me2 (Fig 4H and I, SI Appendix, Fig S8 and S10A).  
333 Interestingly, the most repressed genes also tend to have the sharpest H3K9me2 increase, which is  
334 particularly true in S-EIs. (Fig 4H, SI Appendix, Fig S10A). To see whether H3K9me2 defect might  
335 affect the expression of EI genes, we generated the quadruple mutant *caa39 suvh456* mutated for  
336 the H3K9 methylase genes *KRYPTONITE (KYP)/ SUVH4, SUVH5* and *SUVH6* and examined the  
337 expression of the seven pericentromeric genes already studied. The expression of some EI genes was  
338 significantly increased in *caa39 suvh456* as compared to *caa39* (Fig S10B). Taken together, these  
339 results suggest that H3K9me2 increase plays a role in the reduced expression of EI genes, although  
340 higher order chromatin structure, changes in other histone modification, and other indirect effects of  
341 the *caa39* mutation may contribute to gene expression changes.

342

### 343 **The Topo VI subunit BIN4 physically associates with MAT3**

344 To gain knowledge on the molecular mechanism by which Topo VI contributes to the  
345 delimitation of chromatin boundaries, we used the BIN4 subunit as a bait to screen a yeast two  
346 hybrid (Y2H) cDNA library (Hybrigenics). A strong interaction with the Topo VI subunit RHL1 was  
347 detected, thereby demonstrating the reliability of the screening procedure (Dataset S6). Among the  
348 eleven additional interacting partners, three proteins belong to the S-AdenosylMethionine (SAM)  
349 biosynthesis pathway, the universal methyl group donor (52). The first one, 5-methylthioribose-1-  
350 phosphate isomerase (MTI1, AT2G05830), is involved in the methionine salvage pathway whereas  
351 the two others, Methionine Synthase 1 (MS1, AT5G17920) and Methionine Adenosyltransferase 3  
352 (MAT3, AT2G36880) are the ultimate enzymes of the SAM cycle. In order to identify BIN4-interacting  
353 proteins *in planta*, we also performed a CoIP-MS experiment using the *Arabidopsis mid-1*

354 *35S:BIN4/MID-YFP* line, which consists of the *mid-1* allelic mutant of *BIN4* complemented with YFP-  
355 tagged BIN4/MID (39), and a wt line as control. To exclude nonspecific proteins, we discarded  
356 proteins that were not detected in both BIN4/MID-YFP CoIP-MS replicates, as well as plastidial,  
357 mitochondrial and peroxisomal proteins. The presence of the RHL1 and TOP6B Topo VI subunits in  
358 BIN4/MID-YFP CoIPs validated our procedure (Dataset S7). Remarkably, MAT3 co-  
359 immunoprecipitated strongly with BIN4. MAT4 also co-immunoprecipitated with BIN4, but  
360 apparently to a much lesser extent (Dataset S7). We further investigated the genetic and biochemical  
361 interactions between BIN4 and enzymes of the SAM cycle, particularly the very last enzyme MAT3,  
362 using Bimolecular Fluorescence Complementation (BiFC). We confirmed the BIN4-MAT3 and BIN4-  
363 MS1 interactions in nuclei of transiently agro-transformed *Nicotiana benthamiana* mesophyll cells  
364 (Fig 5A).

365

### 366 **MAT3 is required for H3K9me2**

367 Given that MAT enzymes synthesize the SAM required for DNA and histone methylation, and  
368 that Topo VI is required for proper distribution of H3K9me2 throughout EI-containing  
369 heterochromatic regions, we hypothesized that disruption of MAT3 affects H3K9me2 deposition. To  
370 address this question, we used a recently characterized knock-down line in which *MAT3* 3'-UTR is  
371 interrupted by a T-DNA (53), generating strongly reduced but still detectable transcripts levels (SI  
372 Appendix, Fig S11A). We measured H3K9me2 levels at the four TEs strongly de-repressed in Topo VI  
373 mutant plants (Fig 2) by ChIP-qPCR and found decreased levels of H3K9me2 (Fig 5B). This modest  
374 decrease of H3K9me2 might be explained by the hypomorphic nature of the mutation or by a  
375 functional redundancy between MAT isoforms that share over 85% amino acid sequence identity (SI  
376 Appendix, Fig S11B). To test this hypothesis, we took advantage of a homozygous, mono-insertional,  
377 co-suppressor transgenic line obtained during the process of generating *MAT3-YFP* overexpressors,  
378 that we referred to as *MAT* KD (Fig 5C, SI Appendix, Fig S11C). Owing to their high DNA sequence  
379 identity (SI Appendix, Fig S11D), all *MAT* genes are downregulated in this line (SI Appendix, Fig S11E).  
380 In addition, the stochastic silencing of *MATs* gives rise to different phenotype severities: mildly  
381 affected *MAT* KD plants (Fig 5C) that accumulate less *MATs* transcripts than wt (SI Appendix, Fig  
382 S11E) and present a more severe phenotype than *mat3* hypomorphic mutant plants (Fig 5C); and  
383 strongly affected *MAT* KD+ sister plants (Fig 5C) that accumulate even less *MAT* transcripts (SI  
384 Appendix, Fig S11E). As anticipated, the H3K9me2 decrease was even more pronounced in *MAT* KD  
385 plants than in *mat3* (Fig 5B). These results suggest that MAT isoforms possibly have additive roles in  
386 H3K9 dimethylation. Given the decrease of H3K9me2 in MAT-deficient plants, we then determined

387 the extent of TE reactivation in *mat3* and *MAT* KD by RT-qPCR analysis of the same four TEs. We  
388 observed increased levels of TE transcripts in *mat3* (Fig 5D). This increase was generally more  
389 pronounced in *MAT* KD plants, particularly in *MAT* KD+ plants (Fig 5D). In contrast, we did not  
390 observe any significant effect on EI gene expression (SI Appendix, Fig S11F).

391

### 392 **Topo VI favors MAT enrichment at some heterochromatin borders and depletion from euchromatic** 393 **islands**

394 Collectively, our results suggest that Topo VI and MAT3 could act together in maintaining  
395 sharp chromatin boundaries by influencing H3K9me2 deposition. We therefore used a newly  
396 developed anti-MAT antibody (Agrisera, Vännäs, Sweden) to test for MAT enrichment at specific loci  
397 and a putative Topo VI dependency. First, the specificity of this antibody was validated by  
398 immunoblot analysis of protein extracts from wt, *MAT* KD and *MAT3-YFP* overexpressing lines (SI  
399 Appendix, Fig S12A). We then performed ChIP-qPCR using an anti-MAT antibody and chromatin from  
400 wt and *caa39* plants, to measure the recovery of TEs that are reactivated upon Topo VI or MATs loss  
401 of functions. Interestingly, MATs were enriched on all the tested TEs in wt and less in *caa39*, as  
402 compared to an IgG negative control (Fig 6A). To specifically evaluate the implication of the BIN4/  
403 MID-associated MAT3 isoform, we performed ChIP-qPCR using an anti-GFP antibody and chromatin  
404 from two independent *MAT3-YFP* expressing lines. TEs reactivated in *MAT* KD and in Topo VI mutant  
405 plants were also specifically enriched in the GFP-pulled down chromatin (SI Appendix, Fig S12B).  
406 These results indicate that Topo VI is required for the association of MAT3 with heterochromatic  
407 elements.

408 To test whether Topo VI might also influence the enrichment of MATs at EIs, we performed  
409 ChIP-qPCR using an anti-MAT antibody and chromatin from wt and *caa39*, and analyzed the same EI  
410 as in Figures 4E and I, which shows increased H3K9me2 levels within the island body (probe 3-4) but  
411 decreased levels in the 5' heterochromatic border (probe 1) in *caa39* (Fig 4E and I, Fig 6B, top panel).  
412 We detected a significant decrease of MAT occupancy in this border in *caa39* (Fig 6B, bottom panel,  
413 probe 1) and, conversely, significantly enhanced MAT occupancy in the island body (probe 3) in  
414 *caa39* compared to wt (Fig 6B, bottom panel, probes 3-4). We analyzed three other S-EIs that show  
415 decreased gene expression levels (Fig 3C), increased internal H3K9me2 levels (Figs 4C and SI  
416 Appendix, Fig S8) and contain a single gene (*At4g06634*'s and *At5g30495*'s EIs) or two genes  
417 (*At2g07340*'s EIs). We observed trends of decreased MAT occupancy at one or both borders and  
418 enhanced MAT occupancy in the island bodies of *caa39* (Fig 6C-E). These results suggest that the loss

419 of Topo VI leads to MAT redistribution over EIs, which correlates with H3K9me2 redistribution and  
420 EIs heterochromatinization in *caa39*.

## 421 Discussion

422 The *Arabidopsis* epigenome is largely indexed by discrete chromatin signatures usually  
423 corresponding to single genetic element (e.g., a gene or a TE) (49, 54). However, despite this, in  
424 *Arabidopsis* DNA methylation has a known tendency to spread away from many TEs (55), and a few  
425 other studies have reported the existence of heterochromatin spreading in plants (56–58). Yet, the  
426 mechanisms that repress heterochromatin spreading, hence safeguarding EIs, are poorly understood  
427 in plants. Our study confirmed the existence of an insulator-like mechanism that preserves EIs and  
428 unveiled the role played by the Topo VI complex in this process. We first provide evidence that Topo  
429 VI is required to preserve the euchromatic nature and transcriptional activity of gene islands within  
430 pericentromeric and chromosome 4 knob heterochromatic regions. Indeed, the most remarkable  
431 effect of the *caa39* mutation was the specific misregulation of pericentromeric elements, with a  
432 general downregulation of EI genes and, inversely, a reactivation of some heterochromatic TEs. We  
433 confirmed this peculiar expression pattern in several amorphic and hypomorphic mutants of the  
434 Topo VI complex. Surprisingly, EI gene downregulation is more pronounced in the hypomorphic  
435 mutants *caa39* and *BIN4* KD than in the corresponding null Topo VI mutants that display more severe  
436 growth defects. Taking advantage of uncoupled growth defects and gene expression changes in the  
437 hypomorphic *caa39* allele, we were able to show that the repression of EI genes is correlated with  
438 the invasion of EIs by H3K9me<sub>2</sub>, indicating that Topo VI is required to prevent the spreading of  
439 H3K9me<sub>2</sub>, here referred to as a boundary function. The increased expression of some EI genes in the  
440 quadruple mutant *caa39 suvh456*, defective for the H3K9 methylase SUVH4, SUVH5 and SUVH6, as  
441 compared with *caa39*, further supported that H3K9me<sub>2</sub> spreading over EI genes participates to some  
442 extent in the transcriptional silencing of EI genes in Topo VI defective plants.

443 Although it is known that CHG methylation is maintained through a feedback loop with  
444 H3K9me<sub>2</sub>, WGBS identified no global increase of cytosine methylation over EIs in *caa39*, but rather a  
445 slight decrease of CHG methylation, suggesting that DNA methylation is not involved in the reduced  
446 expression of EI genes in Topo VI mutants. Other recent work has also shown that, under specific  
447 circumstances, increased H3K9me<sub>2</sub> levels do not necessarily result in increased CHG or CHH  
448 methylation, and vice versa. For instance, the AT-hook protein AHL10 ectopically recruits H3K9me<sub>2</sub>  
449 to small, AT-rich TEs without coincidental increase in DNA methylation (59). Conversely, the  
450 expression of *AtCMT3* in *Eutrema Salsugineum*, a Brassicaceae that has lost *CMT3* and gene body  
451 methylation, induces *de novo* gene body methylation in CHG, CHH and CG contexts, but without  
452 resulting in stable gain of H3K9me<sub>2</sub>. Interestingly, CHG hypermethylation in gene bodies is also not  
453 correlated with consistent changes in gene expression in this case (60). While DNA methylation does  
454 not appear to be involved in the reduced expression of EI genes in Topo VI mutants, the question of



455 the relative importance of H3K9me2 remains. Indeed, and firstly, the level of H3K9me2 in EIs of  
456 *caa39* is still significantly lower than in canonical heterochromatin. This might result from histone H3  
457 demethylation, a process that is likely still active in *caa39*. Alternatively, gain of H3K9me2 could be  
458 the outcome of a subset of cells in which *caa39* mutation has a strong effect on H3K9me2  
459 boundaries. Secondly, the negative correlation between EI gene expressions and H3K9me2 changes is  
460 good, particularly in small EIs, but not very high, suggesting that H3K9me2 spreading over EI genes  
461 cannot entirely explain the transcriptional silencing of EI genes. H3K9me2 spreading on EIs might, in  
462 turn, affect the establishment of other chromatin modifications. For instance, in the *ibm1* mutant,  
463 increased levels of H3K9me2 on gene bodies are associated with decreased levels of H3K4me1 and  
464 transcriptional silencing (61). Conversely, in the *svh456* triple mutant, many TEs show a drastic  
465 increase in H3K4me1 level, which is associated with transcriptional derepression and loss of  
466 H3K9me2 (61). Therefore, it is plausible that other histone methylation changes also occur in *caa39*,  
467 as we did observe for H3K27me3, which shows an opposite trend to H3K9me2 in EIs. Thus, H3K9me2  
468 spreading might itself perturb H3K27me3 deposition by PRC2 and/or erasing by trithorax group (trxG)  
469 proteins. This second hypothesis is supported by similar observations made in other organisms,  
470 where the loss of Swi6/HP1 leads to H3K9me2 spreading across natural constitutive heterochromatin  
471 boundaries in fission yeast (62), and alters H3K27me3 deposition on facultative heterochromatin in  
472 *Neurospora crassa* (63).

473 In animals, insulator proteins like CTCF can participate in several distinct processes, e.g.  
474 locally as a chromatin barrier and more globally on the formation of topologically associating  
475 domains (64). Similarly, the disorganization of chromocenters and the partial loss of pericentromeric  
476 TE silencing observed in Topo VI mutants might result from the loss of a local boundary function and,  
477 possibly, also by the loss of a distinct, more global, architectural function of Topo VI in  
478 heterochromatin condensation. Indeed, given that no obvious loss of DNA methylation and only a  
479 partial decrease of H3K9me2 over TEs were observed in Topo VI mutant plants, the reactivation of  
480 TEs is unlikely to be solely explained by decreased levels of these marks, but rather by a combined  
481 loosening of their heterochromatic nature and of their higher order organization. Although causal link  
482 between chromatin reorganization and TEs reactivation in plants is very disputed, a few recent  
483 studies link chromatin organizers with TE derepression independently of DNA demethylation. For  
484 instance, the natural depletion of histone 1 in sex cells is responsible of the reactivation of approx.  
485 100 heterochromatic TEs via DNA demethylation-dependent (77/98) and -independent (21/98)  
486 mechanisms (65). In addition, MORC proteins, which belong to the GHKL ATPases superfamily like  
487 Topo VI, are required for the silencing of approx. 20 TEs and the formation of chromocenters without  
488 impacting H3K9me2 and DNA methylation levels (66–68). Interestingly human CTCF has been shown

489 to interact with Topo II $\beta$  (69, 70) and appears to be part of a protein interaction network that also  
490 contains MORC2 and members of the cohesin complex in HeLa cells (71). Intriguingly, plant and  
491 human recombinant MORC proteins seem to display a type II topoisomerase-like activity, which  
492 requires additional plant extracts for full activity (72).

493         Given the function of MAT enzymes in the synthesis of SAM, MAT perturbation is expected to  
494 affect a wide range of methylation reactions, which include DNA and histone methylations. The *mat3*  
495 mutant line used in our study has been shown, however, to have global SAM levels similar to wt and  
496 only very slightly reduced global levels of DNA methylations, unlike other *mat* mutants that show  
497 more severe DNA and histone methylation defects (73). This suggests that the increased levels of  
498 some TE transcripts in *mat3*, and the corresponding decreased levels of H3K9me<sub>2</sub>, are more likely  
499 attributable to a local effect of the *mat3* mutation, rather than a global decrease of SAM, or be the  
500 outcome of a subset of cells in which *mat3* mutation has a strong effect. Our finding that the Topo VI  
501 BIN4 subunit directly interacts with MAT3 and is required for MAT3 enrichment at some TE loci and  
502 depletion from euchromatic islands, might provide a mechanistic explanation for such a local role of  
503 MAT3 on chromatin, in addition to its general role in SAM synthesis (73). Similarly, the mammal  
504 MATII $\alpha$  isoform also directly supplies SAM in the close vicinity of oncogenes to allow transcriptional  
505 repression and H3K9me<sub>2</sub> deposition (74, 75). Intriguingly, the mouse MATII $\alpha$  has been found to  
506 interact with Topoisomerase II $\alpha$ , a type IIA topoisomerase whose C-terminal regulatory domain  
507 possesses sequence similarity with the BIN4 subunit of the plant Topo VI complex (38). Hence,  
508 although this requires testing in other organisms, an interaction between MAT enzymes and type II  
509 topoisomerases might be evolutionary conserved. Targeting of MATs to specific chromatin regions by  
510 topoisomerases might be a way to couple SAM synthesis and availability *in situ*, possibly for DNA or  
511 histone methylation. Extensive genome-wide studies will provide a general view of chromatin  
512 modification changes in different *mat* mutants and their relative impacts on TE and gene expression.

513         In plants, the existence of an insulator-like function that would partition chromatin into  
514 different functional domains has long been questioned (9, 11, 26). We show that Topo VI participates  
515 to such a function by preventing the spreading of the heterochromatic mark H3K9me<sub>2</sub> into  
516 neighboring euchromatin islands. Our results suggest that the prevention of heterochromatin  
517 spreading might rely upon a Topo VI-MAT3 interaction that would be important for the proper  
518 targeting of MAT3 to heterochromatin and its exclusion from euchromatic islands. Future studies  
519 might allow the identification of direct molecular links between Topo VI, MAT proteins and  
520 methyltransferases involved in DNA and histone methylation, for fine-tuning the establishment of  
521 sharp transitions in chromatin identity along the genome.

## 522 **Materials and Methods**

523 Detailed descriptions of the experimental methods are provided in SI Appendix, Supplementary  
524 Materials and Methods. These include cloning procedures, plant material and growth conditions,  
525 DNA preparation, Chop- and CHIP-qPCR, anti-5-meC ELISA assay, yeast two-hybrid screen, co-  
526 immunoprecipitation-MS, Western blot, RNA extraction, RT-qPCR and microarrays, RNA-seq library  
527 preparation and sequencing, RNA-seq bioinformatic treatment and analysis, whole-genome bisulfite  
528 sequencing and DNA methylation analysis, chromatin immunoprecipitation, CHIP-seq analysis,  
529 immunofluorescence, transient transformation and protoplasts preparation, confocal and  
530 epifluorescence microscopy.

531

## 532 **Availability of data and material**

533 CHIP-seq, RNA-seq, BS-seq and microarray datasets are available at  
534 <https://www.ncbi.nlm.nih.gov/geo/query/acc.cgi?acc=GSE103924> (reviewer token:  
535 slchuqakvwwfpsi). Custom scripts used in this study are available at [https://github.com/michel-](https://github.com/michel-teresse)  
536 [teresse](https://github.com/michel-teresse).

537

## 538 **Acknowledgments**

539 We thank Imen Mestiri (IBENS, Paris) for her expertise with cytogenetics. We also want to express  
540 our gratitude to students who contributed to this work, especially Justine Quillet, Julien Vieu and  
541 César Botella. We thank Ben Field for critical reading of the manuscript. This work was supported by  
542 the French National Research Agency (ANR 2010-JCJC-1205-01 and ANR-14-CE02-0010 to CL). Work  
543 by FB was supported by the Investissements d'Avenir LabexMemory in Living Systems (MEMOLIFE)  
544 grant ANR-10-LABX-54. LD was supported by CEA and Région PACA. High-throughput RNA-  
545 sequencing was performed at the POPS platform, supported by the LabEx Saclay Plant Sciences-SPS  
546 (ANR-10-LABX-0040-SPS). MS analysis was performed at the IMM platform supported by a grant  
547 from GIS IBiSA. High-throughput CHIP-seq was performed at the TGML platform, supported by grants  
548 from Inserm, GIS IBiSA, Aix-Marseille Université, and ANR-10-INBS-0009-10.

549

## 550 **Author contributions**

551 LVM, FV, CV, LD, MR, and CB performed the experiments. CL and MT performed the bioinformatic  
552 analyses. LST was in charge of the sequencing. LVM, CL, FB and CL analyzed the data. LVM, KS, FB and  
553 CL designed the research. LVM, FB and CL wrote the manuscript. All authors read and approved the  
554 final manuscript.

555

## 556 **Conflict of interest**

557 The authors declare that they have no conflict of interest

558

559

## 560 **References**

- 561 1. J. Wang, S. T. Lawry, A. L. Cohen, S. Jia, Chromosome boundary elements and regulation of  
562 heterochromatin spreading. *Cell. Mol. Life Sci.* **71**, 4841–4852 (2014).
- 563 2. H. J. Muller, Types of visible variations induced by X-rays in *Drosophila*. *J. Genet.* **22**, 299–334  
564 (1930).
- 565 3. T. Ali, R. Renkawitz, M. Bartkuhn, Insulators and domains of gene expression. *Curr. Opin.*  
566 *Genet. Dev.* **37**, 17–26 (2016).
- 567 4. W. A. Bickmore, B. van Steensel, Genome Architecture: Domain Organization of Interphase  
568 Chromosomes. *Cell* **152**, 1270–1284 (2013).
- 569 5. J. Dekker, T. Misteli, Long-Range Chromatin Interactions. *Cold Spring Harb. Perspect. Biol.* **7**,  
570 a019356 (2015).
- 571 6. J. R. Dixon, *et al.*, Topological domains in mammalian genomes identified by analysis of  
572 chromatin interactions. *Nature* **485**, 376–380 (2012).
- 573 7. B. Bonev, G. Cavalli, Organization and function of the 3D genome. *Nat. Rev. Genet.* **17**, 772–  
574 772 (2016).
- 575 8. P. Heger, B. Marin, M. Bartkuhn, E. Schierenberg, T. Wiehe, The chromatin insulator CTCF and  
576 the emergence of metazoan diversity. *Proc. Natl. Acad. Sci.* **109**, 17507–17512 (2012).
- 577 9. C. Wang, *et al.*, Genome-wide analysis of local chromatin packing in *Arabidopsis thaliana*.  
578 *Genome Res.* **25**, 246–256 (2015).

- 579 10. S. D. Singer, J. M. Hily, K. D. Cox, Analysis of the enhancer-blocking function of the TBS  
580 element from *Petunia hybrida* in transgenic *Arabidopsis thaliana* and *Nicotiana tabacum*.  
581 *Plant Cell Rep.* **30**, 2013–2025 (2011).
- 582 11. C. Liu, Y.-J. Cheng, J.-W. Wang, D. Weigel, Prominent topologically associated domains  
583 differentiate global chromatin packing in rice from *Arabidopsis*. *Nat. Plants* **3**, 742–748 (2017).
- 584 12. C. Liu, D. Weigel, Chromatin in 3D: progress and prospects for plants. *Genome Biol.* **16**, 170  
585 (2015).
- 586 13. J. Sequeira-Mendes, C. Gutierrez, Genome architecture: from linear organisation of chromatin  
587 to the 3D assembly in the nucleus. *Chromosoma* **125**, 455–469 (2016).
- 588 14. S. Grob, M. W. Schmid, N. W. Luedtke, T. Wicker, U. Grossniklaus, Characterization of  
589 chromosomal architecture in *Arabidopsis* by chromosome conformation capture. *Genome*  
590 *Biol.* **14**, R129 (2013).
- 591 15. S. Grob, M. W. Schmid, U. Grossniklaus, Hi-C Analysis in *Arabidopsis* Identifies the KNOT , a  
592 Structure with Similarities to the flamenco Locus of *Drosophila*. *Mol. Cell* **55**, 678–693 (2014).
- 593 16. S. Feng, *et al.*, Genome-wide Hi-C Analyses in Wild-Type and Mutants Reveal High-Resolution  
594 Chromatin Interactions in *Arabidopsis*. *Mol. Cell* **55**, 694–707 (2014).
- 595 17. A. Veluchamy, *et al.*, LHP1 Regulates H3K27me3 Spreading and Shapes the Three-Dimensional  
596 Conformation of the *Arabidopsis* Genome. *PLoS One* **11**, e0158936 (2016).
- 597 18. C. Liu, *et al.*, Genome-wide analysis of chromatin packing in *Arabidopsis thaliana* at single-  
598 gene resolution. *Genome Res.* **26**, 1057–1068 (2016).
- 599 19. P. Fransz, H. De Jong, From nucleosome to chromosome: A dynamic organization of genetic  
600 information. *Plant J.* **66**, 4–17 (2011).
- 601 20. L. Simon, M. Voisin, C. Tatout, A. V. Probst, Structure and function of centromeric and  
602 pericentromeric heterochromatin in *Arabidopsis thaliana*. *Front. Plant Sci.* **6**, 1–8 (2015).
- 603 21. S. Del Prete, J. Arpón, K. Sakai, P. Andrey, V. Gaudin, Nuclear Architecture and Chromatin  
604 Dynamics in Interphase Nuclei of *Arabidopsis thaliana*. *Cytogenet. Genome Res.* **143**, 28–50  
605 (2014).
- 606 22. P. Fransz, J. H. de Jong, M. Lysak, M. R. Castiglione, I. Schubert, Interphase chromosomes in  
607 *Arabidopsis* are organized as well defined chromocenters from which euchromatin loops  
608 emanate. *Proc. Natl. Acad. Sci.* **99**, 14584–14589 (2002).

- 609 23. W. J. J. Soppe, *et al.*, DNA methylation controls histone H3 lysine 9 methylation and  
610 heterochromatin assembly in Arabidopsis. *EMBO J.* **21**, 6549–6559 (2002).
- 611 24. O. Mathieu, A. V Probst, J. Paszkowski, Distinct regulation of histone H3 methylation at lysines  
612 27 and 9 by CpG methylation in Arabidopsis. *EMBO J.* **24**, 2783–2791 (2005).
- 613 25. Z. Lippman, *et al.*, Role of transposable elements in heterochromatin and epigenetic control.  
614 *Nature* **430**, 471–476 (2004).
- 615 26. Z. Vergara, C. Gutierrez, Emerging roles of chromatin in the maintenance of genome  
616 organization and function in plants. *Genome Biol.* **18**, 96 (2017).
- 617 27. A. Bergerat, D. Gabelle, P. Forterre, Purification of a DNA topoisomerase II from the  
618 hyperthermophilic archaeon *Sulfolobus shibatae*. A thermostable enzyme with both bacterial  
619 and eucaryal features. *J. Biol. Chem.* **269**, 27663–27669 (1994).
- 620 28. A. Bergerat, *et al.*, An atypical topoisomerase II from archaea with implications for meiotic  
621 recombination. *Nature* **386**, 414–417 (1997).
- 622 29. K. Schneider, *et al.*, The ROOT HAIRLESS 1 gene encodes a nuclear protein required for root  
623 hair initiation in Arabidopsis. *Genes (Basel)*. **12**, 2013–2021 (1998).
- 624 30. K. Schneider, B. Wells, L. Dolan, K. Roberts, Structural and genetic analysis of epidermal cell  
625 differentiation in Arabidopsis primary roots. *Development* **124**, 1789–1798 (1997).
- 626 31. K. Sugimoto-Shirasu, *et al.*, RHL1 is an essential component of the plant DNA topoisomerase  
627 VI complex and is required for ploidy-dependent cell growth. *Proc. Natl. Acad. Sci. U. S. A.*  
628 **102**, 18736–41 (2005).
- 629 32. H. J. Yoon, *et al.*, Lotus japonicus SUNERGOS1 encodes a predicted subunit A of a DNA  
630 topoisomerase VI that is required for nodule differentiation and accommodation of rhizobial  
631 infection. *Plant J.* **78**, 811–821 (2014).
- 632 33. F. Hartung, H. Puchta, Molecular characterization of homologues of both subunits A (SPO11)  
633 and B of the archaeobacterial topoisomerase 6 in plants. *Gene* **271**, 81–86 (2001).
- 634 34. F. Hartung, *et al.*, An archaeobacterial topoisomerase homolog not present in other eukaryotes  
635 is indispensable for cell proliferation of plants. *Curr. Biol.* **12**, 1787–1791 (2002).
- 636 35. Y. Yin, *et al.*, A crucial role for the putative Arabidopsis topoisomerase VI in plant growth and  
637 development. *Proc. Natl. Acad. Sci. U. S. A.* **99**, 10191–6 (2002).

- 638 36. A. Mittal, *et al.*, TOPOISOMERASE 6B is involved in chromatin remodelling associated with  
639 control of carbon partitioning into secondary metabolites and cell walls, and epidermal  
640 morphogenesis in Arabidopsis. *J. Exp. Bot.* **65**, 4217–4239 (2014).
- 641 37. K. Sugimoto-shirasu, N. J. Stacey, J. Corsar, K. Roberts, M. C. Mccann, DNA Topoisomerase VI  
642 Is Essential for Endoreduplication in Arabidopsis. *Curr. Biol.* **12**, 1782–1786 (2002).
- 643 38. C. Breuer, *et al.*, BIN4, a Novel Component of the Plant DNA Topoisomerase VI Complex, Is  
644 Required for Endoreduplication in Arabidopsis. *Plant Cell* **19**, 3655–3668 (2007).
- 645 39. V. Kirik, A. Schrader, J. F. Uhrig, M. Hulskamp, MIDGET unravels functions of the Arabidopsis  
646 topoisomerase VI complex in DNA endoreduplication, chromatin condensation, and  
647 transcriptional silencing. *Plant Cell* **19**, 3100–3110 (2007).
- 648 40. E. L. Meczes, K. L. Gilroy, K. L. West, C. a Austin, The Impact of the Human DNA  
649 Topoisomerase II C-Terminal Domain on Activity. *PLoS One* **3**, e1754 (2008).
- 650 41. A. Onoda, *et al.*, Nuclear dynamics of topoisomerase II $\beta$  reflects its catalytic activity that is  
651 regulated by binding of RNA to the C-terminal domain. *Nucleic Acids Res.* **42**, 9005–9020  
652 (2014).
- 653 42. K. L. Gilroy, C. A. Austin, The Impact of the C-Terminal Domain on the Interaction of Human  
654 DNA Topoisomerase II  $\alpha$  and  $\beta$  with DNA. *PLoS One* **6**, e14693 (2011).
- 655 43. Y. Pommier, Y. Sun, S.-Y. N. Huang, J. L. Nitiss, Roles of eukaryotic topoisomerases in  
656 transcription, replication and genomic stability. *Nat. Rev. Mol. Cell Biol.* **17**, 703–721 (2016).
- 657 44. M. Jain, A. K. Tyagi, J. P. Khurana, Overexpression of putative topoisomerase 6 genes from rice  
658 confers stress tolerance in transgenic Arabidopsis plants. *FEBS J.* **273**, 5245–5260 (2006).
- 659 45. M. Jain, A. K. Tyagi, J. P. Khurana, Constitutive expression of a meiotic recombination protein  
660 gene homolog, OsTOP6A1, from rice confers abiotic stress tolerance in transgenic Arabidopsis  
661 plants. *Plant Cell Rep.* **27**, 767–778 (2008).
- 662 46. K. Simkova, *et al.*, Integration of stress-related and reactive oxygen species-mediated signals  
663 by Topoisomerase VI in Arabidopsis thaliana. *Proc. Natl. Acad. Sci.* **109**, 16360–16365 (2012).
- 664 47. C. J. Underwood, I. R. Henderson, R. A. Martienssen, Genetic and epigenetic variation of  
665 transposable elements in Arabidopsis. *Curr. Opin. Plant Biol.* **36**, 135–141 (2017).
- 666 48. K. De Preter, R. Barriot, F. Speleman, J. Vandesompele, Y. Moreau, Positional gene enrichment  
667 analysis of gene sets for high-resolution identification of overrepresented chromosomal

- 668 regions. *Nucleic Acids Res.* **36**, 1–6 (2008).
- 669 49. J. Sequeira-Mendes, *et al.*, The Functional Topography of the Arabidopsis Genome Is  
670 Organized in a Reduced Number of Linear Motifs of Chromatin States. *Plant Cell* **26**, 2351–  
671 2366 (2014).
- 672 50. L. Shen, *et al.*, diffReps: Detecting Differential Chromatin Modification Sites from ChIP-seq  
673 Data with Biological Replicates. *PLoS One* **8**, e65598 (2013).
- 674 51. H. Stroud, *et al.*, Non-CG methylation patterns shape the epigenetic landscape in Arabidopsis.  
675 *Nat. Struct. Mol. Biol.* **21**, 64–72 (2014).
- 676 52. P. Zhang, MetaCyc and AraCyc. Metabolic Pathway Databases for Plant Research. *Plant*  
677 *Physiol.* **138**, 27–37 (2005).
- 678 53. Y. Chen, T. Zou, S. McCormick, S -Adenosylmethionine Synthetase 3 Is Important for Pollen  
679 Tube Growth. *Plant Physiol.* **172**, 244–253 (2016).
- 680 54. F. Roudier, *et al.*, Integrative epigenomic mapping defines four main chromatin states in  
681 Arabidopsis. *EMBO J.* **30**, 1928–1938 (2011).
- 682 55. I. Ahmed, A. Sarazin, C. Bowler, V. Colot, H. Quesneville, Genome-wide evidence for local DNA  
683 methylation spreading from small RNA-targeted sequences in Arabidopsis. *Nucleic Acids Res.*  
684 **39**, 6919–6931 (2011).
- 685 56. S. R. Eichten, *et al.*, Spreading of Heterochromatin Is Limited to Specific Families of Maize  
686 Retrotransposons. *PLoS Genet.* **8**, e1003127 (2012).
- 687 57. Z. Lang, *et al.*, The Methyl-CpG-Binding Protein MBD7 Facilitates Active DNA Demethylation to  
688 Limit DNA Hyper-Methylation and Transcriptional Gene Silencing. *Mol. Cell* **57**, 971–983  
689 (2015).
- 690 58. H. Saze, A. Shiraishi, A. Miura, T. Kakutani, Control of Genic DNA Methylation by a jmjC  
691 Domain-Containing Protein in Arabidopsis thaliana. *Science (80-. )*. **319**, 462–465 (2008).
- 692 59. H. Jiang, *et al.*, Ectopic application of the repressive histone modification H3K9me2  
693 establishes post-zygotic reproductive isolation in Arabidopsis thaliana. *Genes Dev.* **31**, 1272–  
694 1287 (2017).
- 695 60. J. M. Wendte, *et al.*, Epimutations are associated with CHROMOMETHYLASE 3-induced de  
696 novo DNA methylation. *Elife* **8** (2019).



- 697 61. S. Inagaki, *et al.*, Gene-body chromatin modification dynamics mediate epigenome  
698 differentiation in *Arabidopsis*. *EMBO J.* **36**, 970–980 (2017).
- 699 62. R. Stunnenberg, *et al.*, H3K9 methylation extends across natural boundaries of  
700 heterochromatin in the absence of an HP1 protein. *EMBO J.* **34**, 2789–2803 (2015).
- 701 63. K. Jamieson, *et al.*, Loss of HP1 causes depletion of H3K27me3 from facultative  
702 heterochromatin and gain of H3K27me2 at constitutive heterochromatin. *Genome Res.* **26**,  
703 97–107 (2016).
- 704 64. Y. Lu, G. Shan, J. Xue, C. Chen, C. Zhang, Defining the multivalent functions of CTCF from  
705 chromatin state and three-dimensional chromatin interactions. *Nucleic Acids Res.* **44**, 6200–  
706 6212 (2016).
- 707 65. S. He, M. Vickers, J. Zhang, X. Feng, Natural depletion of histone H1 in sex cells causes DNA  
708 demethylation, heterochromatin decondensation and transposon activation. *Elife* **8**, 1–23  
709 (2019).
- 710 66. G. Moissiard, *et al.*, MORC family ATPases required for heterochromatin condensation and  
711 gene silencing. *Science* **336**, 1448–51 (2012).
- 712 67. Z. J. Lorkovi, U. Naumann, A. J. M. Matzke, M. Matzke, Involvement of a GHKL ATPase in RNA-  
713 Directed DNA Methylation in *Arabidopsis thaliana*. *Curr. Biol.* **22**, 933–938 (2012).
- 714 68. T. R. Brabbs, *et al.*, The stochastic silencing phenotype of *Arabidopsis morc6* mutants reveals a  
715 role in efficient RNA -directed DNA methylation. *Plant J.* **75**, 836–846 (2013).
- 716 69. M. Witcher, B. M. Emerson, Epigenetic Silencing of the p16INK4a Tumor Suppressor Is  
717 Associated with Loss of CTCF Binding and a Chromatin Boundary. *Mol. Cell* **34**, 271–284  
718 (2009).
- 719 70. T. M. Yusufzai, H. Tagami, Y. Nakatani, G. Felsenfeld, CTCF Tethers an Insulator to Subnuclear  
720 Sites, Suggesting Shared Insulator Mechanisms across Species. *Mol. Cell* **13**, 291–298 (2004).
- 721 71. L. Uusküla-reimand, *et al.*, Topoisomerase II beta interacts with cohesin and CTCF at  
722 topological domain borders. *Genome Biol.* **17**, 1–22 (2016).
- 723 72. M. Manohar, *et al.*, Plant and human MORC proteins have DNA modifying activities similar to  
724 type II topoisomerases, but require additional factor(s) for full activity. *Mol. Plant. Microbe.*  
725 *Interact.* **30**, 87–100 (2017).
- 726 73. J. Meng, *et al.*, METHIONINE ADENOSYLTRANSFERASE4 Mediates DNA and Histone

- 727 Methylation. *Plant Physiol.* **177**, 652–670 (2018).
- 728 74. Y. Katoh, *et al.*, Methionine Adenosyltransferase II Serves as a Transcriptional Corepressor of  
729 Maf Oncoprotein. *Mol. Cell* **41**, 554–566 (2011).
- 730 75. Y. Kera, *et al.*, Methionine Adenosyltransferase II-dependent Histone H3K9 Methylation at the  
731 COX-2 Gene Locus. *J. Biol. Chem.* **288**, 13592–13601 (2013).
- 732 76. H. Thorvaldsdóttir, J. T. Robinson, J. P. Mesirov, Integrative Genomics Viewer (IGV): High-  
733 performance genomics data visualization and exploration. *Brief. Bioinform.* **14**, 178–192  
734 (2013).
- 735

736 **Figure legends**

737 **Figure 1. Topoisomerase VI is required for heterochromatin organization.** (A) Representative  
738 nucleus ( $n > 30$ ) from 6-day-old wt and *caa39* cotyledon epidermal cells stained with DAPI and  
739 showing indirect immunolocalization of H3K9me2. Scale bar: 5  $\mu\text{m}$ . (B) Two independently prepared  
740 nuclear extracts of wt and *caa39* were immunoblotted against H3 or H3K9me2, as indicated. (C)  
741 Same as (A) for 5-meC localization. (D) Elisa assay to quantify total 5-meC in 6-day-old cotyledons of  
742 wt, *caa39* and *ddm1-8*. \*\*:  $P < 0.005$  (Student's *t*-test).

743

744 **Figure 2. Topo VI is required for the silencing of transposable elements.** (A) Bar chart showing the  
745 proportions of reactivated TE superfamilies in *caa39* compared to the general proportion of TEs in  
746 the genome. The relative percentage is shown for each superfamily and the absolute number of  
747 reactivated TEs is noted above each bar. \*\*:  $P < 0.005$ ; \*\*\*\*:  $P < 0.0001$  (Chi-squared test). (B) RT-  
748 qPCR confirmation of the reactivation of selected TEs in *caa39*, *rhl2-1* and *bin4-1*. Error bars:  $\pm$  SEM  
749 of three biological replicates. \*:  $P < 0.05$ ; \*\*:  $P < 0.005$ ; \*\*\*:  $P < 0.0005$  (Student's *t*-test). (C) DNA  
750 from indicated genotypes were extracted and digested with McrBC. The mean ratio of digested over  
751 undigested DNA from three biological replicates is shown. Error bars:  $\pm$  SEM of three biological  
752 replicates. \*:  $P < 0.05$ ; \*\*:  $P < 0.005$ ; \*\*\*:  $P < 0.0005$  (Student's *t*-test). (D) Average distribution of  
753 methylated cytosine in CG, CHG and CHH contexts over TEs and 2 kb flanking regions. Two  
754 independent replicates for each genotype were performed. (E) CHIP-qPCR of H3K9me2 at selected  
755 TEs. Error bars:  $\pm$  SEM of three biological replicates. \*:  $P < 0.05$ ; \*\*:  $P < 0.005$ ; \*\*\*:  $P < 0.0005$   
756 (Student's *t*-test). (F) Average distribution of H3-normalized H3K9me2 over TEs and 2 kb flanking  
757 regions. Two (H3) and three (H3K9me2) independent biological replicates for each genotype were  
758 performed.

759

760 **Figure 3. Genes in euchromatic islands within heterochromatic pericentromeric and chromosome 4**  
761 **knob regions are repressed in Topo VI mutants.** (A) Positional Gene Enrichment (PGE) analysis of the  
762 top 500 most downregulated genes in *caa39*. The bed files corresponding to coordinates of the  
763 widest enriched regions ( $\text{FDR} < 0.05$ ) were visualized with a genome browser. Black lines correspond  
764 to enriched regions, blue boxes correspond to pericentromeric regions as defined by Yelina et al.  
765 (2012), green box to the knob and red to centromeres. (B) Scatter plots and Pearson correlations of  
766 differentially expressed ( $P < 0.05$ ) pericentromeric genes in *caa39* and *bin4-1* or *bin4-2*. (C) RT-qPCR  
767 of selected pericentromeric genes in *caa39*, *rhl2-1*, *bin4-1* and *BIN4* KD at 6 days post-germination.  
768 Error bars:  $\pm$  SEM of three biological replicates. \*\*:  $P < 0.005$ ; \*\*\*:  $P < 0.0005$ ; \*\*\*\*:  $P < 0.0001$  (two-

769 way ANOVA, Dunnett's test). (D) The proportion of each chromatin state was computed for EIs and  
770 their 1.5 kb flanking regions. EI: Euchromatic Islands. (E) Gene content in EIs.

771

772 **Figure 4. Topo VI prevents the invasion of euchromatic islands by H3K9me2.** (A) ChIP-qPCR analysis  
773 of H3K9me2 at EI genes. Error bars:  $\pm$  SEM of two biological replicates. \*:  $P < 0.05$ ; \*\*\*:  $P < 0.0005$ ;  
774 \*\*\*\*:  $P < 0.0001$  (two-way ANOVA, Fisher's test). (B) Average distribution of H3-normalized  
775 H3K9me2 along short euchromatic gene islands and 4 kb flanking regions. Two (H3) and three  
776 (H3K9me2) independent biological replicates for each genotype were performed.  $P$ -value was  
777 computed for each aggregated point by using the Mann-Whitney test. (C) Same as (B) long EIs. (D)  
778 Bar chart showing the average percentage of down or up H3K9me2 peaks identified by diffReps  
779 analysis in the genome, EIs, EI genes (EIGs), EI gene body, 5' and 3' UTRs. Error bars:  $\pm$ SEM of three  
780 biological replicates. \*:  $P < 0.05$ ; \*\*\*:  $P < 0.0005$ ; \*\*\*\*:  $P < 0.0001$  (two-way ANOVA, Fisher's test). (E)  
781 ChIP-qPCR validation of a single-gene island for H3K9me2. Error bars:  $\pm$ SEM of three biological  
782 replicates. \*:  $P < 0.05$ ; \*\*\*\*:  $P < 0.0001$  (two-way ANOVA, Fisher's test). (F) Average distribution of  
783 methylated cytosine in CG, CHG and CHH contexts over EIs. Two independent replicates for each  
784 genotype were performed. (G) K-means linear clustering of H3K9me2 and H3K27me3 tag densities  
785 across EIs and their 900 nt flanking borders as revealed by seqMINER in *caa39* and wt. (H) Heatmap  
786 correlation clustering of EI genes with significant changes in RNA-seq and H3K9me2/H3 ChIP-seq. (I)  
787 Integrative Genomics Viewer (76) screenshot of H3, H3K9me2, H3K27me3, RNA, CG, CHG and CHH  
788 methylation profiles in wt and *caa39* on a single gene-containing island. Each track is normalized  
789 against corresponding input samples (ChIP-seq) and by the sequencing depth. Numbers indicate the  
790 position of primers used in (E).

791

792 **Figure 5. MAT3 interacts with Topo VI and is required for H3K9me2 deposition on heterochromatic**  
793 **loci.**

794 (A) Protoplasts from transiently agrotransformed *N. benthamiana* leaves expressing different  
795 combination of BiFC vectors, as indicated. Nuclei were stained with Hoechst 33342. (B) Chromatin of  
796 3 week-old wt or *MAT* KD (here a mixed pool of *MATs* silenced plants with strong or weak  
797 phenotype) rosette leaves, or 6 day-old wt or *mat3* cotyledon nuclei was immunoprecipitated with  
798 anti-H3K9me2 antibodies and the recovery of TEs known to be reactivated in *caa39* was assessed by  
799 qPCR. The result is shown as a percentage of recovery normalized against wt. Error bars:  $\pm$  SEM of  
800 two biological replicates. \*:  $P < 0.05$ ; \*\*:  $P < 0.005$ ; \*\*\*:  $P < 0.0005$ ; \*\*\*\*:  $P < 0.0001$  (two-way  
801 ANOVA, Dunnett's test). (C) Representative photographs of 4-week-old wt, *MATs* silenced plants with

802 stronger (*MAT* KD+) and weaker (*MAT* KD) developmental phenotypes, and the *mat3* mutant. (D) RT-  
803 qPCR analysis of TE transcript abundance in indicated genotypes. Error bars:  $\pm$  SEM of three biological  
804 replicates. \*:  $P < 0.05$ ; \*\*:  $P < 0.005$ ; \*\*\*:  $P < 0.0005$  (Student's *t*-test).

805

806 **Figure 6. Topo VI is required for MAT enrichment at heterochromatin borders and exclusion from**  
807 **euchromatic islands.** (A) Chromatin of 6-day-old wt or *caa39* cotyledon nuclei was  
808 immunoprecipitated with anti-MATs antibodies and the recovery of TEs reactivated in *MATs* silenced  
809 plants and *caa39* was measured by qPCR. Error bars:  $\pm$  SEM of three biological replicates. (B-E) Top  
810 panels: Integrative Genomics Viewer screenshots of H3- and sequencing depth-normalized H3K9me2  
811 profiles, and locations of primers used in bottom panels. Bottom panels: Same as (A) on EIs  
812 containing repressed genes in *caa39* such as *AT1G41830* (B), *AT4G06634* (C), *AT2G07340* (D) and  
813 *AT5G30495* (E). Error bars:  $\pm$  SEM of two biological replicates. \*:  $P < 0.05$ ; \*\*:  $P < 0.005$ ; \*\*\*:  $P <$   
814  $0.0005$  (Student's *t*-test).

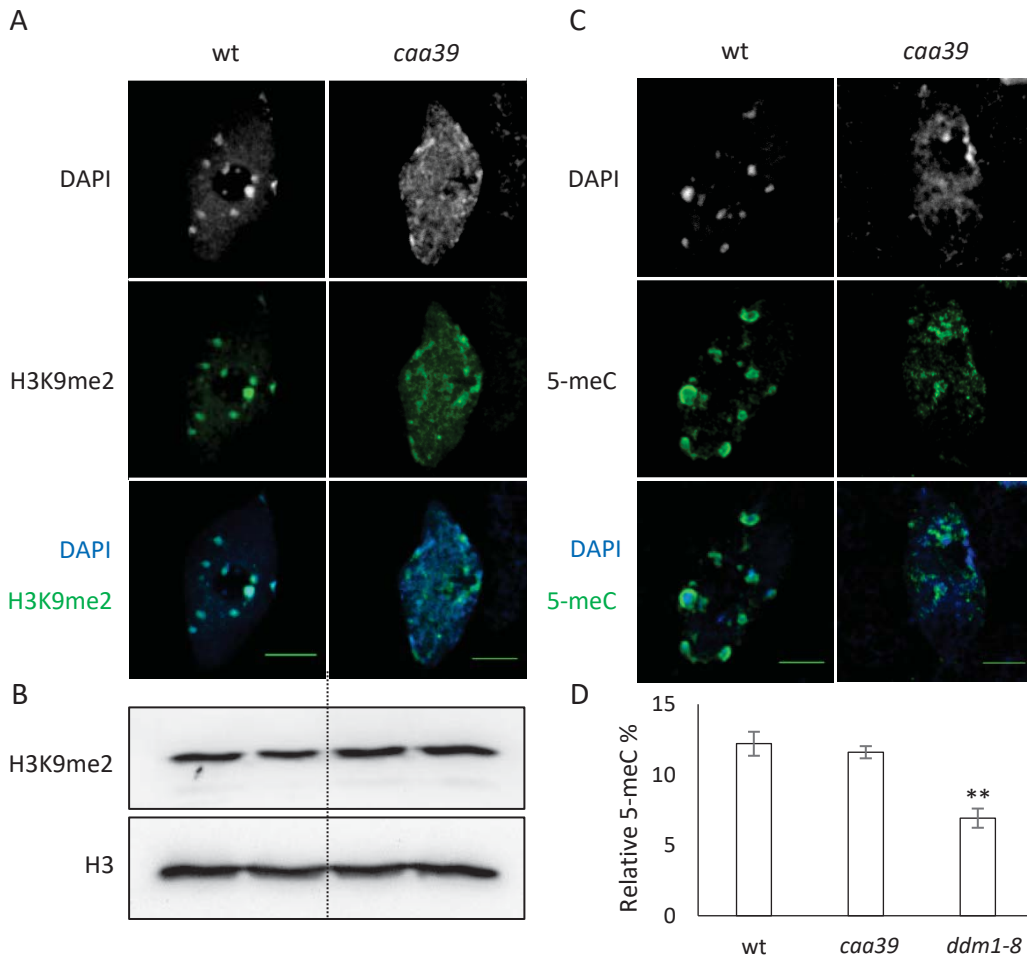


Fig 1

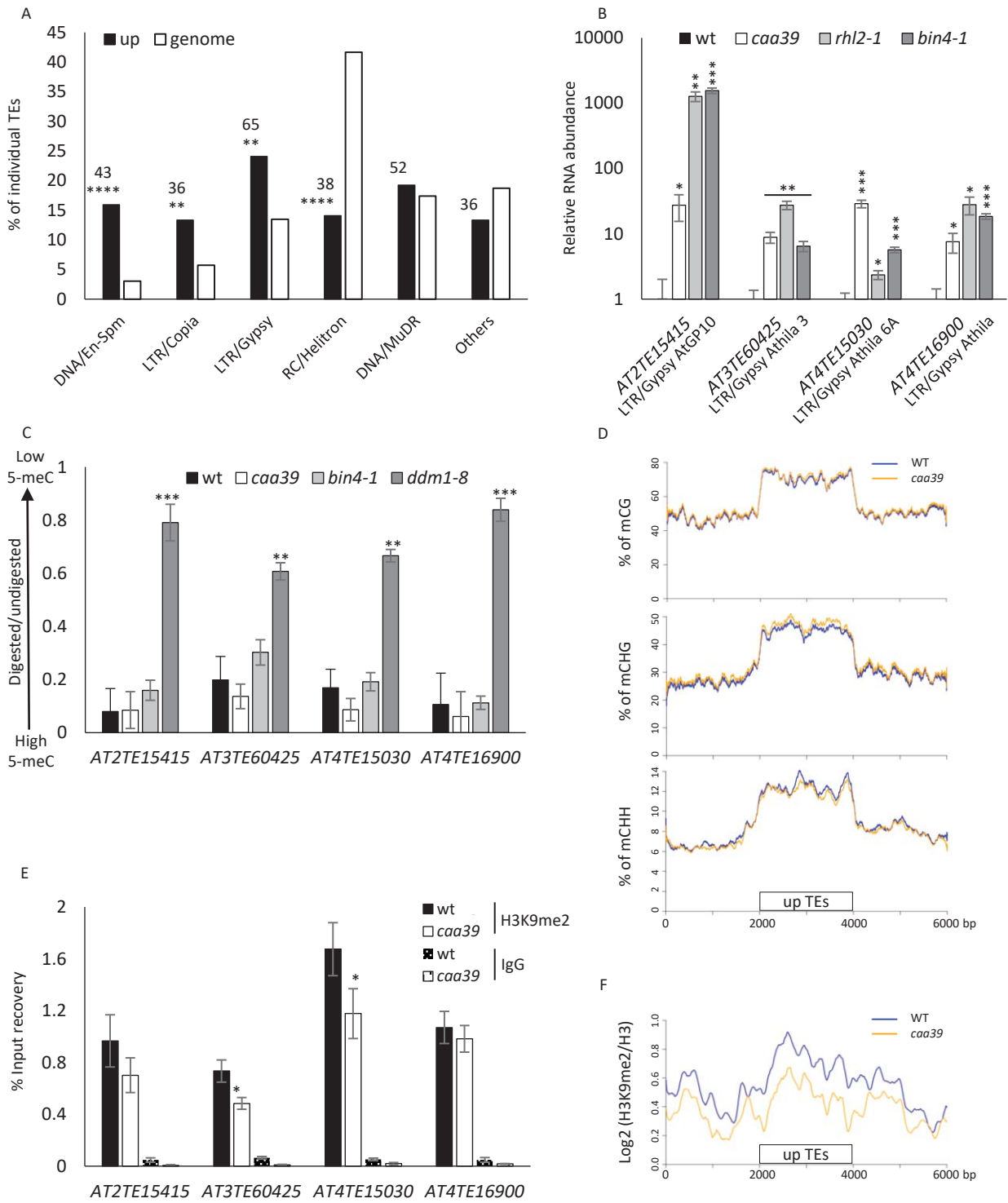


Fig 2

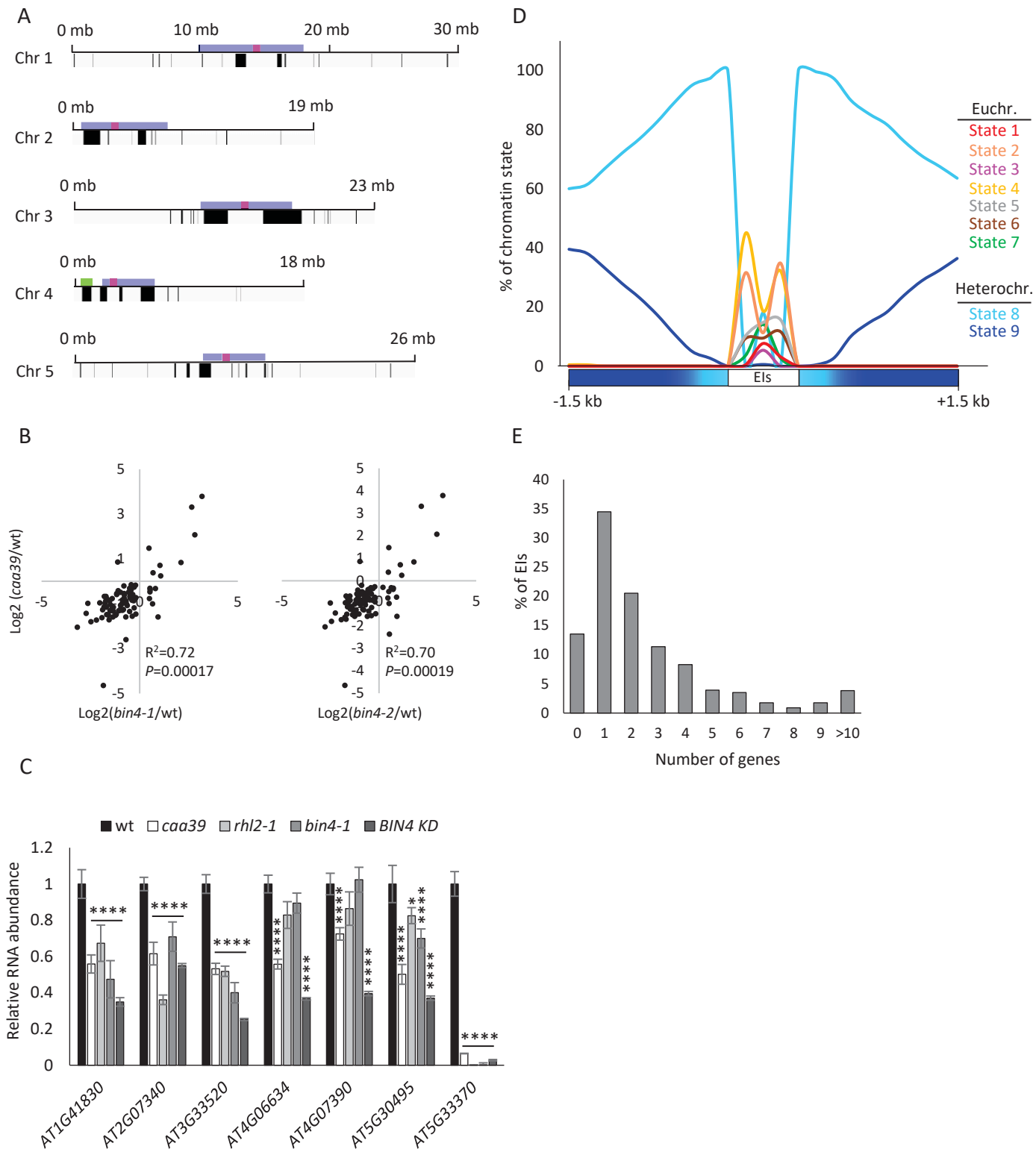


Fig 3



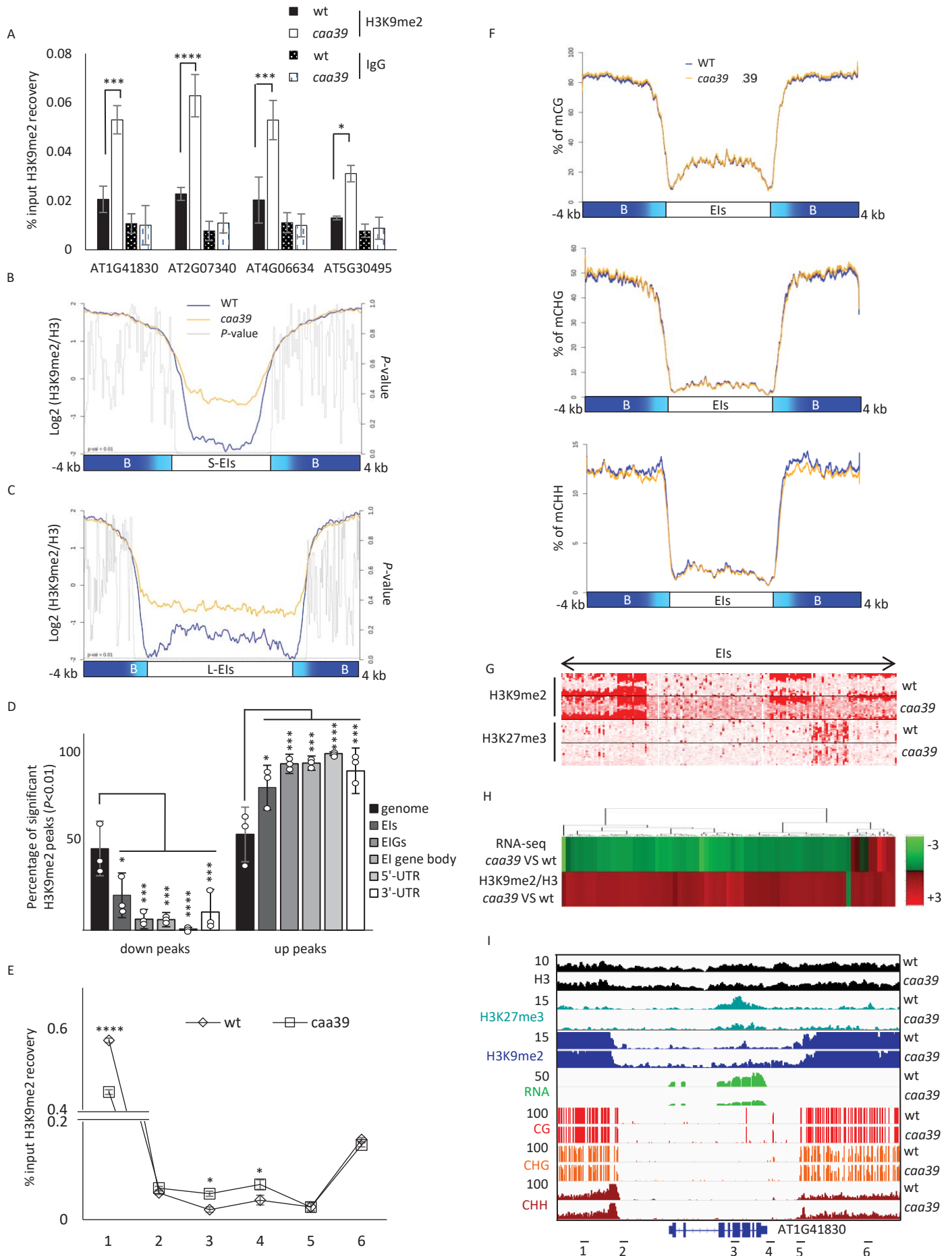


Fig 4

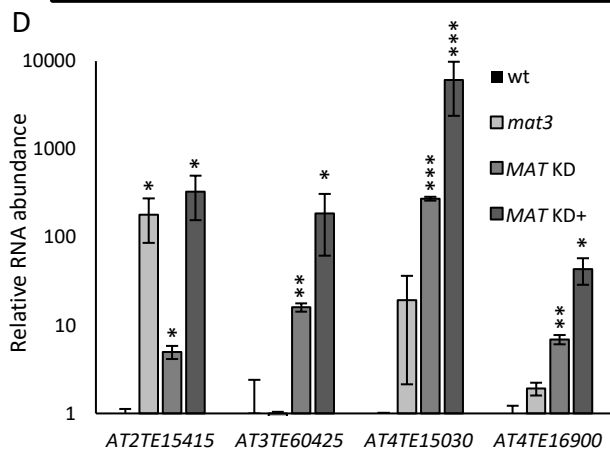
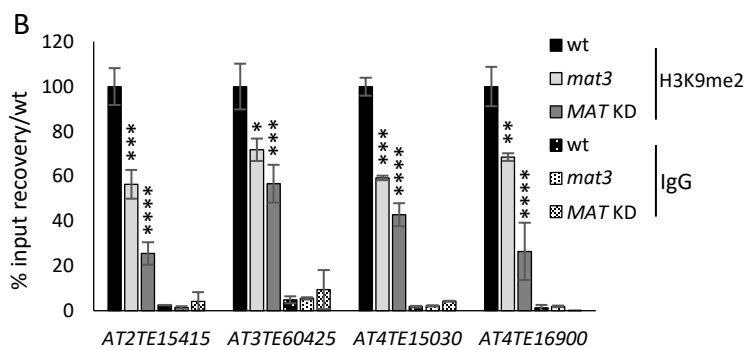
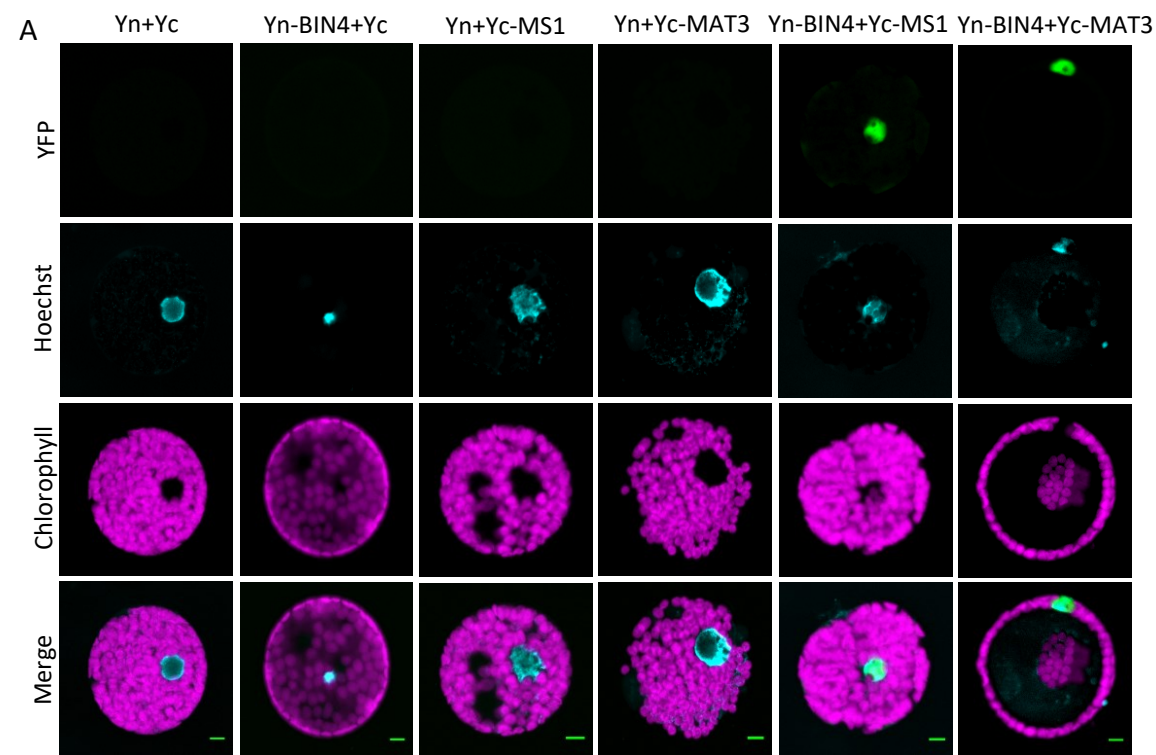


Fig 5

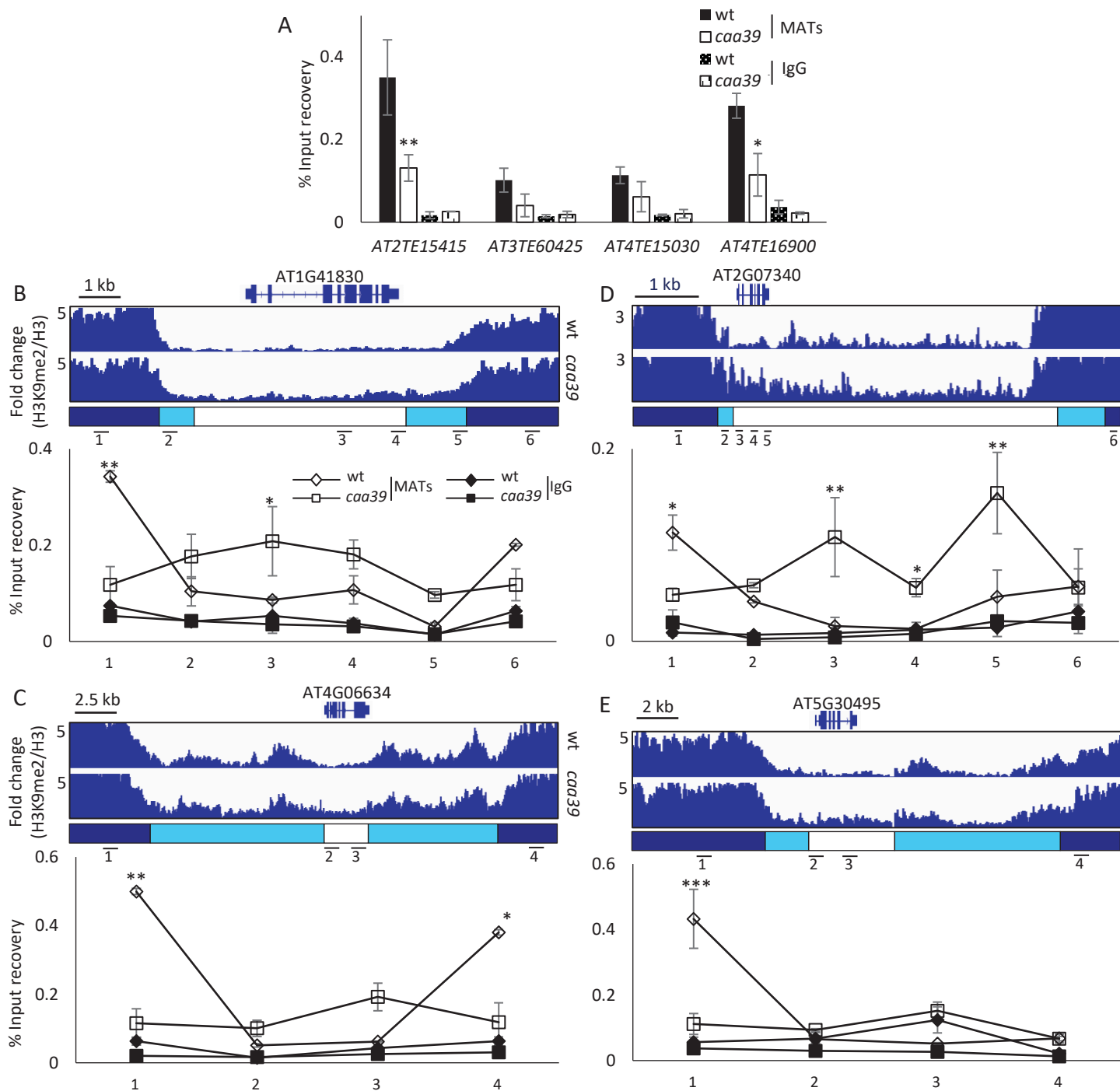


Fig 6